

International Conference on Space Optics—ICSO 2018

Chania, Greece

9–12 October 2018

Edited by Zoran Sodnik, Nikos Karafolas, and Bruno Cugny



Modelization, measurement and correction of a cross-talk image ghost in the Ingenio/SEOSAT payload

C. Miravet

C. Santos

D. Zorita

D. Gil-Leyva

et al.



ics0 proceedings



Modelization, measurement and correction of a cross-talk image ghost in the Ingenio/SEOSAT payload

C. Miravet ^{*a}, C.Santos^a, D. Zorita^a, D. Gil-Leyva^a, I. Cabeza^b, A. Marini^c, F. Reina^c, V. Kirschner^c,
A. Popescu^c

^aSENER Ingeniería y Sistemas, C/Severo Ochoa 4, PTM, Tres Cantos, 28760 Madrid, Spain;

^bAIRBUS Defence and Space, Avda. de Aragón 404, 28022 Madrid, Spain;

^cESTEC-ESA, postbus 299, Keplerlaan 1, 2200 AG Noordwijk, The Netherlands

ABSTRACT

Ingenio/SEOSAT is a high-spatial-resolution optical mission developed under the Spanish Earth Observation National Program for Satellites (PNOTS), and managed technically in the framework of an ESA contract. It features as Primary Payload (PP) a high-resolution optical payload with one 2.5 meter resolution panchromatic channel and four 10 meter resolution visible/near infrared spectral channels. It is based on a twin Korsch telescope concept, each telescope covering half of the instrument's swath width. In this communication is presented a detailed account of the work performed to accurately characterize and correct by post-processing an image ghost present in the multi-spectral channels of the primary payload. The work reported here includes the description and analysis of the results of three test campaigns, performed at Thales Alenia Space. Tests carried out include radiometric tests at focal plane level, generic stray-light tests and a novel test to characterize specifically the parameters of the studied cross-talk image ghost. Field-dependent point spread functions for the studied image ghost have been generated by optical analysis, and have been adjusted with the results of the performed tests. From these, image filters have been devised to reproduce, and remove by subtraction, the image ghost. Quantitative image ghost correction results on an actual test image are shown.

Keywords: Ingenio/SEOSAT, Korsch telescope, stray-light, image ghost, optical cross-talk

1. INTRODUCTION

Ingenio/SEOSAT is a high-spatial-resolution optical mission developed under the Spanish Earth Observation National Program for Satellites (PNOTS), and managed technically in the framework of an ESA contract. It features as Primary Payload (PP) a high-resolution optical payload with one 2.5 meter resolution panchromatic channel and four 10 meter resolution visible/near infrared spectral channels. It is based on a twin Korsch telescope concept, each telescope covering half of the instrument's swath width. In this communication is presented a detailed account of the work performed to accurately characterize and correct by post-processing an image ghost present in the multi-spectral channels of the primary payload. In section 2 is presented a brief description of the Ingenio/SEOSAT primary payload, including focal plane architecture. In section 3 are described the two ray paths originating the studied cross-talk image ghost. The main ghost path (associated to a first reflection on a detector line) level is critically dependent on the along-track alignment between detector and filter, inducing a difference in the measured ghost levels in both cameras. In section 4 are presented the results of the performed cross-talk radiometric characterization tests, devoted to verify the existence of the predicted ghost and to quantify its magnitude. In section 5 are presented the results of generic stray-light tests and a modification of those tests to enable a direct characterization of the image ghost parameters. In section 6 is presented the work performed to generate the image filter that models the image ghost at a point in the field. Finally, in section 7 are presented the results of applying this filter to reproduce and then subtract the image ghost from one of the images acquired during the generic stray-light measurements.

*carlos.miravet@sener.es; www.ingenieriaconstruccion.sener

2. INGENIO/SEOSAT PRIMARY PAYLOAD

Ingenio/SEOSAT¹⁻⁶ features a Primary Payload (PP) with one 2.5 meter resolution panchromatic (PAN) channel and four 10 meter resolution multi-spectral (MS) channels, located respectively in the blue (B), green (G), red (R), and near-infrared (NIR) spectral regions. The payload is equipped with two identical cameras, each covering half of the instrument's swath width of 55 Km. In figure 1 is displayed a CAD model view of the payload (left panel), together with an image of the actual flight model (central panel). In the right panel, it is shown an image of the payload, covered with thermal blankets, acquired during the thermal test campaign at INTA facilities.

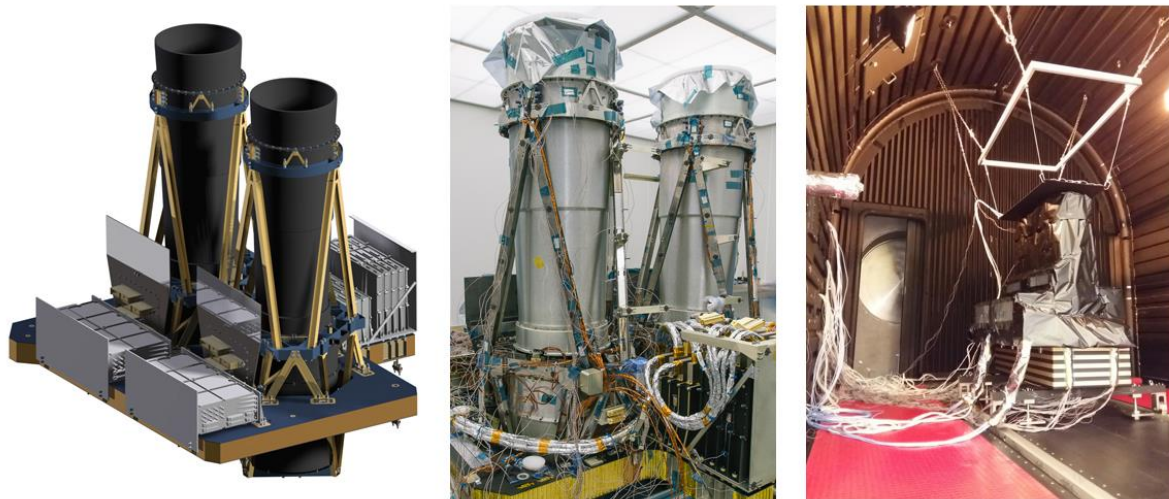


Figure 1. Ingenio/SEOSAT principal payload. Left: CAD model; center: flight model; right: flight model, covered with thermal blankets, during the thermal test campaign.

The camera's optical subsystem is constituted by two identical all-reflective Korsch-type telescopes. In figure 2 (left panel) is presented an optical layout of the telescope. The system is composed of three conical on-axis mirrors plus a plane folding mirror, to redirect the image to the location of the focal plane (FP), in the upper part of the drawing. The telescope output is constituted by four image stripes, corresponding to the four slits cut on the primary mirror (at the center of the image), which act as field diaphragms of the telescope.

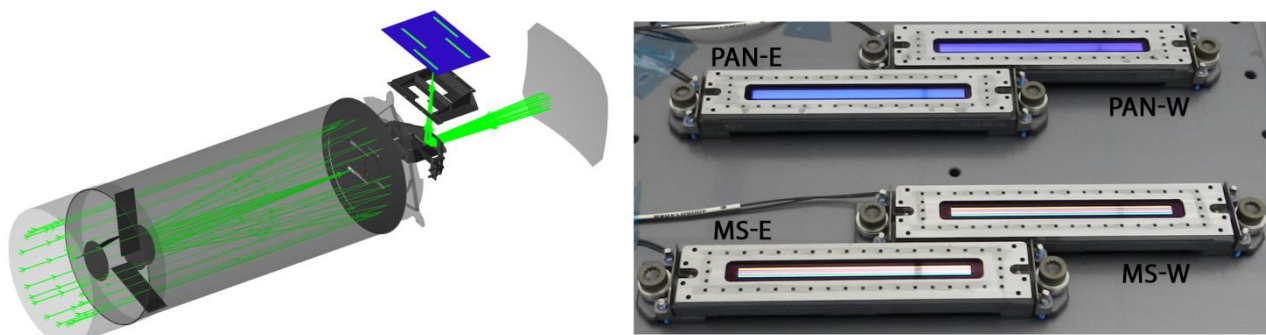


Figure 2. Left: Korsch telescope optical design; right: focal plane assembly, with two PAN and two MS detectors. 'E' and 'W' stand in the figure for east and west, respectively.

In the right panel of figure 2 is presented an image of the focal plane assembly. It is composed of two panchromatic (PAN) and two multi-spectral (MS) detectors, co-planarly located. Detectors on both channels are of CCD type. The detectors used for the PAN channel are based on the Time Delay and Integration (TDI) technology to increase the number of generated photo-electrons, with the corresponding increase in signal-to-noise ratio. A 4-line CCD detector has

been used to implement the MS channels, with each line devoted to sense one of the B, G, R and NIR bands. Each PAN and MS detector is mounted on its proper sub-assembly, which includes the filters defining the spectral bands and the corresponding proximity electronics.

This paper describes the modelization, measurement and correction of a cross-talk image ghost originated by parasitic reflections on the optical elements of the MS-E detector assembly.

3. MS FILTER CROSS-TALK GHOST PATHS

In figure 3 is depicted a diagram of the optical layout of a MS detector assembly. The CCD surface, with its four identical sensing lines, lies at the bottom of the picture. A black mineral coating covers the CCD surface around the sensing lines. For illustration purposes, each line has been represented in the figure with the color of its spectral channel, with magenta having been used in this paper for NIR. On top of the CCD surface, we find the detector window, with a thickness of 1.1 mm and anti-reflection coatings deposited on both sides. Finally, on top of the assembly lies the MS filter, defining the spectral range to be sensed by each CCD line. The telescope side of this element is equipped with four band-pass stripe interference filters, effectively determining the sensed spectral ranges. Regions around the filter lines are coated with a black absorber. On the detector side, the regions containing the ray footprints are coated with a blocker (rendered in brown in the figure), a broad-band transmission filter used to block secondary transmittance bands in the telescope-side filters, while maintaining a high transmittance in the four defined spectral bands. As in the telescope side, a black absorber coating has been deposited around blocker lines.

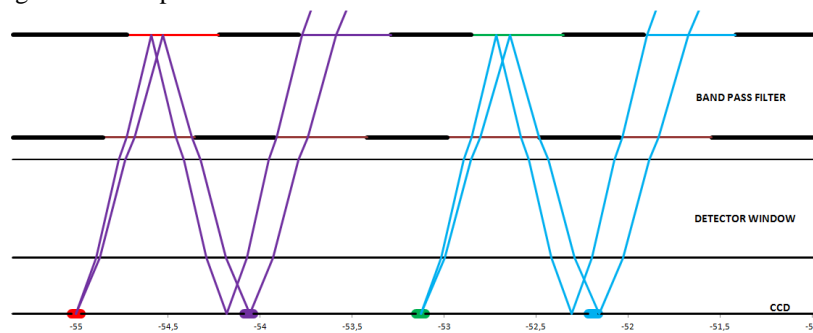


Figure 3. Diagram showing the MS filter optical layout, together with ray paths corresponding to the studied cross-talk image ghost in the MS-E detector.

Figure 3 also displays the ray paths of the studied image ghost, for rays entering the focal plane assembly through the blue and NIR spectral band-pass filters. Rays going through the green spectral filter, not depicted in the figure for clarity, cause a similar effect on the NIR detector. The ghost path is created in all cases by a parasitic reflection on the CCD surface, combined with a second reflection on the following band-pass filter, ending up on the detector line next to the nominal one. These are optical cross-talk paths. By virtue of them, part of the light filtered by the blue spectral filter ends up on the detector line corresponding to the green channel. In the same way, green filtered light illuminates the NIR detector line, and NIR light the red one. The blue CCD line is free of this ghost, as expected from the geometrical layout. There are other possible ghost paths on the MS filter, but this is by far the most energetic, due to the high reflectivity of the band-pass filter to light outside its transmittance band.

As can be seen in the figure, the first reflection on the CCD surface could occur either at a CCD detector line or at the black coating surrounding it. These two paths have different spectral efficiencies, light distributions and tolerances to misalignments, and have to be addressed separately on modelization and analysis. The most energetic path, associated to a first reflection on a detector line, will be referred here as ghost path G_1 . Ghost path G_2 will be in turn associated to a first reflection on the detector black coating.

The described ghost affects in principle only the MS-E detector. In the MS-W detector, rays arrive at a smaller elevation/along-track angle, not reaching the next detector line in nominal conditions, under the shown ghost paths. The rest of the paper addresses in detail the study of the presented cross-talk paths on the MS-E detector.

4. CROSS-TALK RADIOMETRIC CHARACTERIZATION TESTS

4.1 Test set-up

Before resorting to more specific characterization means, a radiometric test was first performed at focal plane level to verify the actual existence of the predicted cross-talk image ghost, and to quantify approximately its magnitude. The set-up employed was based on the one developed by Thales Alenia Space Spain for radiometric tests at FP level, with the focal plane in front of an integrating sphere with aperture matching the diameter and location of the telescope exit pupil. In this way, we managed to reproduce approximately the incidence angles arriving to the detector once integrated into the telescope. In the left and central panels of figure 4 could be seen a diagram and an image of the actual set-up used for these tests, respectively. To quantify the cross-talk image ghost effect, the FP has to be illuminated with a light spectrum contained exclusively in one MS spectral band, so that only one detector line is illuminated nominally. Signals produced by the other detector lines could then be used directly to quantify the magnitude of existing cross-talk effects. In our set-up, this was achieved by placing conveniently at the sphere aperture a 5" witness of one of the MS band-pass filters.



Figure 4. Diagram (left) and image (center) of the used FP radiometric set-up; right: optical FP model corresponding to this test configuration.

4.2 Results prediction and sensitivity analysis

In the right panel of figure 4 is presented a layout of the FP optical model, in this specific test configuration. This model has been used to compute the expected light distribution at the CCD surface, for nominal and ghost image paths. In figure 5 are presented the computed light footprints at the CCD surface corresponding to the nominal path (left panel) and G_1 (center panel) and G_2 (right panel) ghost paths. As can be seen, both ghost footprints are clearly thinner than that of the nominal path due to severe beam vignetting caused by the narrow slits around the stripe filters, at both sides of the filter window.

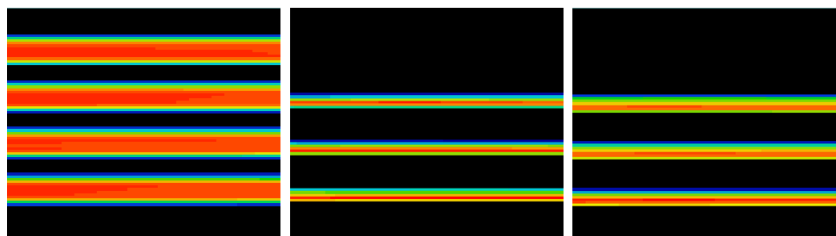


Figure 5. Computed light footprints at the MS CCD surface. Left: nominal; center: G_1 ghost path; right: G_2 ghost path.

A sensitivity analysis has been conducted to assess the stability of ghost levels with respect to small misalignments between the FP optical elements, as could occur during the integration of this equipment. In particular, it has been examined the sensitivity of ghost levels with respect to relative tilts and decenters of the filter window with respect to the CCD surface, for the two studied ghost paths. The results obtained show that ghost levels are relatively stable with respect to small misalignments, but for filter-CCD decenters in the along-track direction (normal to the detector lines), which cause a remarkable effect on the level associated to the G_1 ghost.

In the left panel of figure 6 are displayed the nominal ghost levels associated to G_1 (solid lines) and G_2 (dashed lines) ghosts, for the different MS spectral bands. The color of each line corresponds to the band experiencing the ghost. As in the rest of the paper, magenta has been used to represent the NIR band. According to this graph, the G_1 ghost level is expected to be in the range from 3% (green) to 5% (NIR), whereas the G_2 ghost level is roughly in the range from 2% (green, NIR) to 4% (red). In the right panel of the figure is shown the corresponding levels after applying a 40 μm along-track decenter between filter and CCD. This relatively small displacement causes the G_1 ghost levels to be almost cancelled, maintaining simultaneously the G_2 ghost levels roughly unaltered. To cause a similar effect on the G_2 ghost levels would require a filter-CCD displacement of around 150 μm , which is outside the integration accuracy margin. This high sensitivity of the G_1 ghost to filter-CCD along-track decenters is considered to be the root cause of the different ghost levels measured in both cameras, as will be detailed in the following sections.

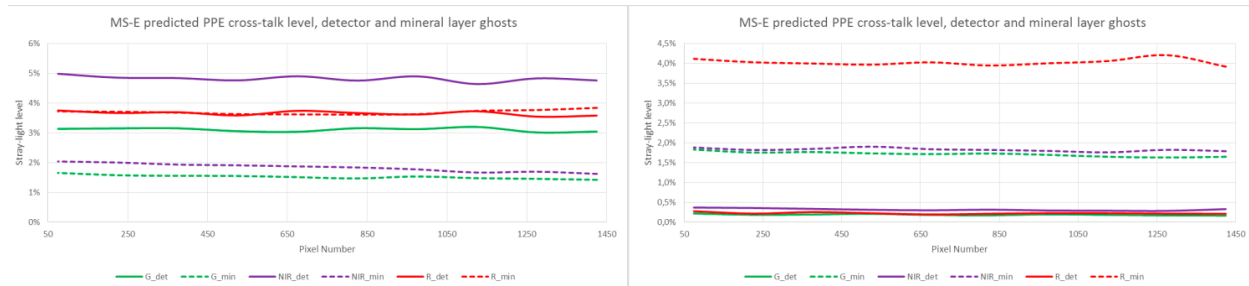


Figure 6. Left: predicted G_1 and G_2 ghost levels in nominal conditions; right: predicted levels for both ghosts after applying a 40 μm along-track decenter between filter and CCD.

4.3 Analysis of results

In figure 7 are presented the results of the performed cross-talk radiometric characterization tests. In the first row are presented the results for the T_1 camera, while the second row is devoted to T_2 camera's results. For each camera are presented three graphs, with the results for the three ghost-affected channels (green, NIR and red). In each graph, the measured ghost level is depicted by a black solid line. The prediction for the level of the G_2 ghost is displayed as a black dotted line. The prediction for the level of the G_1 ghost is displayed as a dotted line with the color of the band originating the ghost (i.e. green for the G_1 ghost affecting the NIR channel). MS-E detector measurements occupy the left side of the graphs.

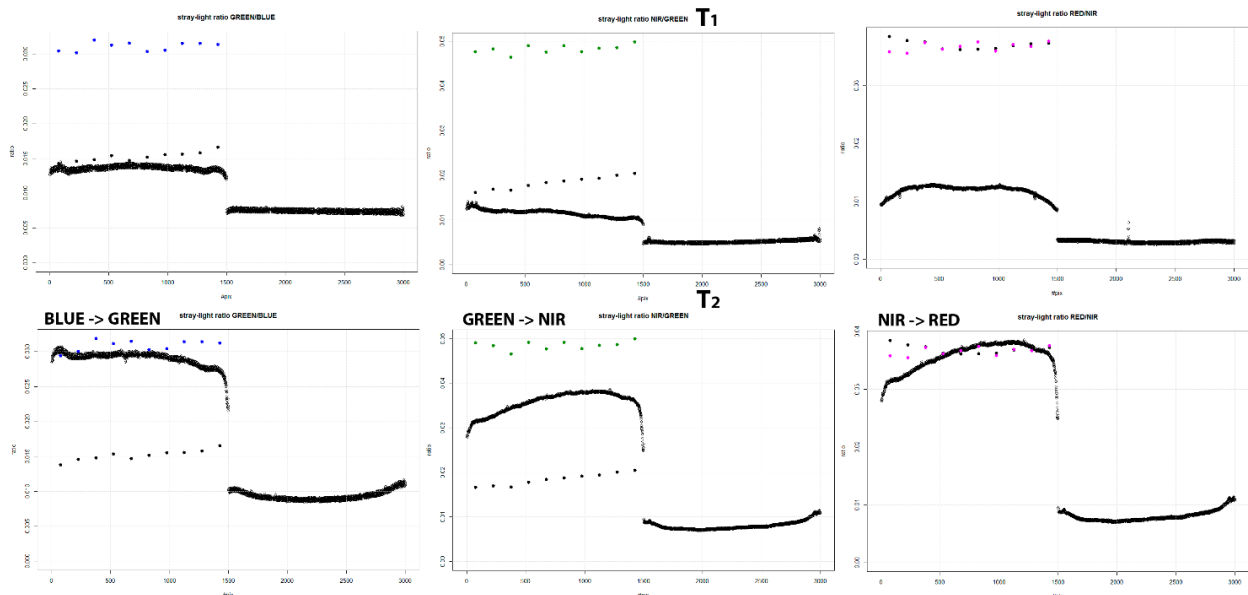


Figure 7. Cross-talk measurements obtained as a result of the performed radiometric characterization tests.

For the green and NIR channels of the T_1 camera, the measurements are roughly coincident with the predictions for the G_2 ghost level. For the T_1 red channel, the measurements are even lower than the prediction for this ghost path, with values similar to that of the other channels. The hypothesis for the observed behavior is that the G_1 ghost is completely absent from this camera, due to its high sensitivity to an across-track decenter between filter and CCD. The lower than predicted values in the red channel are considered to be due to a less than nominal spectral efficiency in that region. The parameter most likely involved is the spectral reflectivity in NIR of the black CCD coating, which has not been measured specifically for the supplied units.

For the T_2 camera, the measured ghost values are in general higher than the ones for the T_1 camera, lying between predictions for G_1 and G_2 ghost paths. The values measured in the red channel are also here lower than in other bands relative to predictions, supporting the assumption of an intrinsic, non-alignment dependent feature. These results could be explained by assuming that the G_1 ghost is partially active in this camera, causing an increase in the measured ghost levels. The assumptions concerning the absence and presence of the G_1 ghost on both cameras has been experimentally verified by means of the specific cross-talk characterization tests, described in section 5.2.

For the T_1 camera, the measured cross-talk values are in the range of 1% to 1.5%. For the T_2 camera, the measured values are larger, in the range of 3% to 4%. These cross-talk values have been refined with the more specialized measurements described in section 5.

5. STRAY-LIGHT CHARACTERIZATION TESTS

5.1 Generic stray-light tests

A set of generic stray-light characterization tests have been performed at camera level, to assess compliance to payload stray-light requirements. For the MS channels, these tests involved the projection of a 75-pix square target at several across-track locations on each MS detector, using a MTF test set-up. In figure 8 is presented a diagram showing the three across-track locations (M_1 , M_2 and M_3) where stray-light levels have been measured on the MS-E detector. M_1 is the location closer to the camera's edge of the field of view.

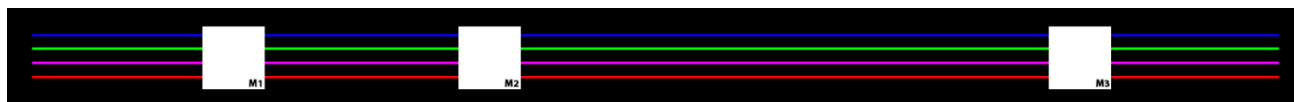


Figure 8. Diagram showing the location of the three across-track positions (M_1 , M_2 and M_3) on the MS-E detector where the 75-pix square target was projected to measure stray-light levels.

At both sides of the square image, the stray-light rejection level was measured at distances from the edge of 2.5, 5 and 10 MS pixels. According to a PP requirement, the measured levels have to be below 4%, 2% and 1%, respectively.

In the left and central panels of figure 9 are presented in a semi-logarithmic plot the normalized results obtained on the left side of the square at field point M_1 in camera T_2 , for the four detector lines. Especially in the red channel, it is apparent the presence of a signal bump around pixel 180, associated to the studied ghost. This effect is also present in other spectral channels, albeit much less notoriously. As predicted by the optical model, the red channel is the most affected one in these tests, due to a combination of two factors: a) The QTH illumination source used in the measurements is biased toward NIR; b) The NIR filter (originating the ghost sensed in the red channel) has the largest bandwidth among the four MS spectral channels. In the right panel of figure 9 are presented the measurements performed at the right side of the square, for blue and red spectral channels. At this side, where the studied ghost is absent, all stray-light rejection levels are below the required values.

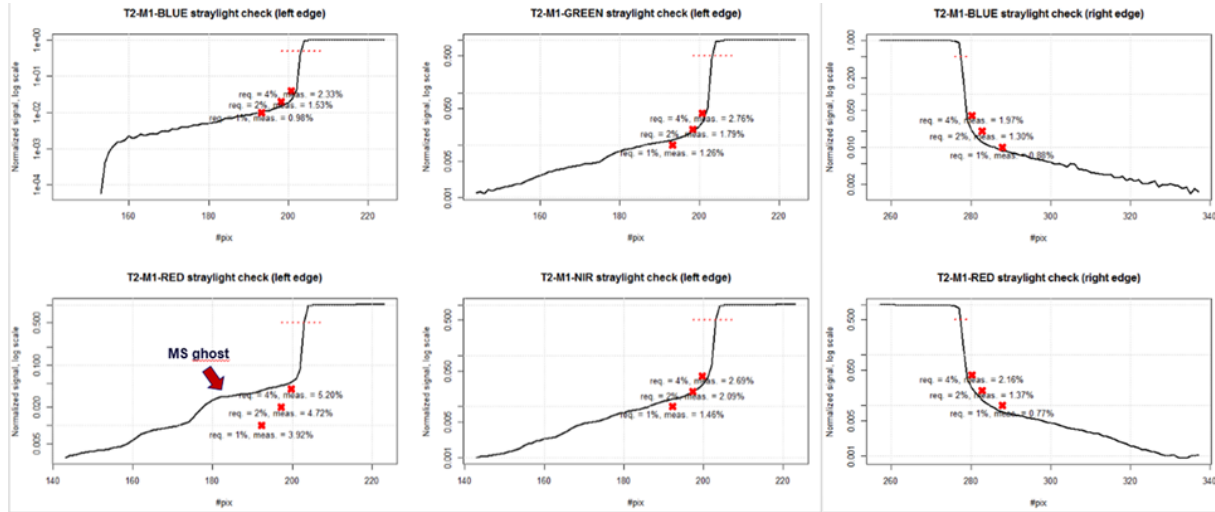


Figure 9. Measured stray-light rejection levels at field point M_1 in camera T_2 .

To compare these stray-light rejection values with the results of the radiometric tests reported in section 4, two operations have to be performed. Firstly, contributions to the stray-light rejection values different from the analyzed ghost have to be removed from the square's left edge signal. Assuming that general stray-light processes affect equally the signal at both sides of the square, this has been approximately performed by subtracting the right edge signal from the left edge signal under study. Secondly, stray-light rejection values have to be referred to the peak signal in the channel causing the ghost, rather than to the peak signal level in the affected channel. Once ghost values are measured with respect to peak values in the band creating the effect, figures for the three bands get remarkably more similar, as predicted by the optical model. For the T_1 camera, the ghost level is roughly around 1%. For the T_2 camera, the ghost level is roughly around a 2%, with NIR values slightly higher (2.5%-3%). The ghost contribution to the measured stray-light level has been further examined with a variation of this test, tailored specifically for optical cross-talk characterization purposes. The obtained results are reported in the following section.

5.2 Specific cross-talk characterization tests

In addition to the performed set of generic stray-light characterization tests, specific cross-talk characterization tests have been carried out with the objective of determining experimentally the magnitude and geometric characteristics of the ghost image generated by the two studied paths. In figure 10 is presented a diagram showing the devised concept. As in the previous test, the MTF bench set-up has been used to project square images at the same three across-track field locations. However, the projected square was in this case substantially smaller (10 MS pixels). At each across-track position, the square image has been displaced at 1-pixel intervals along-track, to acquire a sequence of 100 images covering with margin the four detector lines. By correlating the evolution of the signal in one band with the ghost signal in the affected line, it is possible to discriminate the relative contribution of both ghost paths.

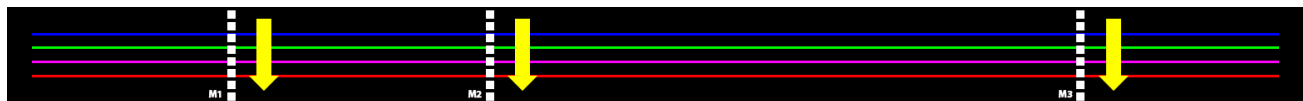


Figure 10. Cross-talk characterization test concept.

In figure 11 are presented the signals acquired in the four spectral channels with the 10-MS square located at across-track point M_1 , in camera T_1 . The data corresponds to along-track position #29 of the total of 100 frames composing the recorded sequence. In the displayed frame, the square image was aligned to the NIR detection line, with the corresponding channel showing a significantly large signal. In the red channel, the largest signal detected corresponds to the studied ghost, almost centered around the predicted location. At its left, corresponding to larger deviation from the

across-track position of the square, a smaller signal was recorded. As the studied ghost corresponds to the largest possible across-track deviation with just two reflections, this second signal is considered to be likely due to a 4-reflection ghost path. Given its low magnitude, its modelization has not been further pursued. At the square across-track location, a faint signal due to general stray-light processes is also apparent in both the green and red channels.

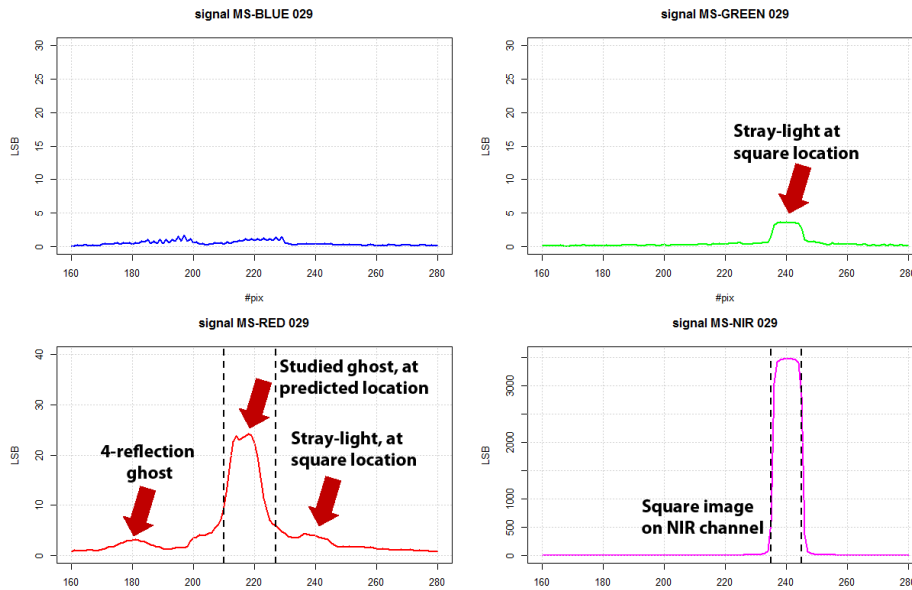


Figure 11. Signals acquired in the four spectral bands with the 10 MS square image centered on the NIR line. T₁-M₁ field point

In figure 12 are displayed, for each frame of the recorded sequence, the peak values in the region occupied by the square in a given channel, together with the peak values in the ghost region predicted by the optical model, in the ghost-affected channel. Both curves are depicted with the color code of the nominal and ghost-affected channel, respectively. In the top row of the picture are presented the results for the cross-talk ghost induced by the green on the NIR channel (left panel) and by the NIR on the red channel (right panel), both in the T₁ camera. As can be seen, there are image frames (#53 for the green-induced ghost and #36-37 for the NIR-induced one) in which the signal in the nominal channel has almost achieved its maximal level (signaling that the detector line in that channel is almost fully illuminated) while the ghost level in the affected channel remains still at very low level. This clearly indicates that the G₁ ghost is practically absent from the T₁ camera. In the bottom row of the picture are presented the corresponding results for the T₂ camera. In this case, it is observed that the increase of the ghost signal is synchronized with that of the nominal square signal on the originating channel, indicating at least a partial presence of the G₁ ghost. As expected, the G₂ ghost is present in both cameras, causing a gradual increase in the ghost level for 2-3 frames after the detector line in the nominal channel has been fully illuminated.

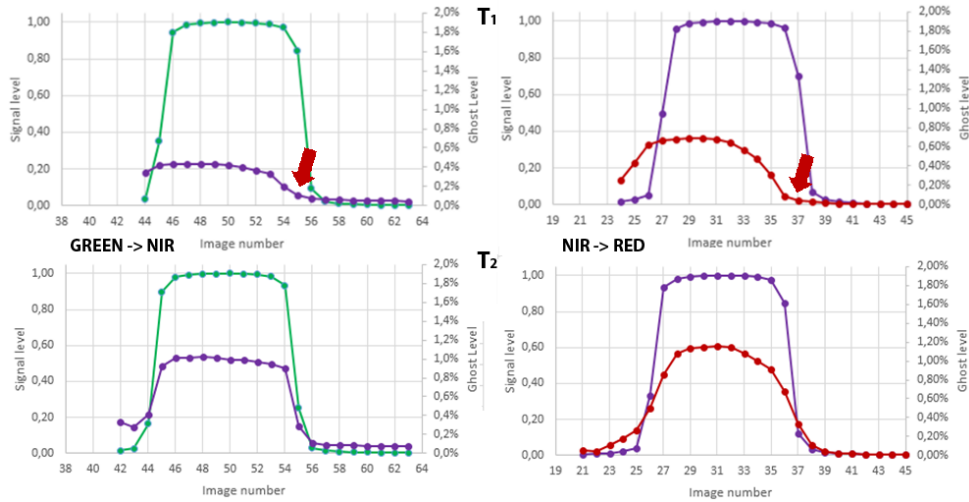


Figure 12. Cross-talk ghost levels, as determined from the specific cross-talk characterization tests.

For the T1 camera, the measured MS filter ghost is around 0.6%-0.7%, from a total 1% ghost contribution measured on the static stray-light tests. For the T2 camera, the measured MS filter ghost is around 1.2%-1.5%, from a total 2% ghost contribution measured on the static stray-light tests. The slightly larger ghost values measured on the NIR band of T2 in the static tests does not appear to be connected to a larger MS filter ghost on that band and camera, according to the specific test results.

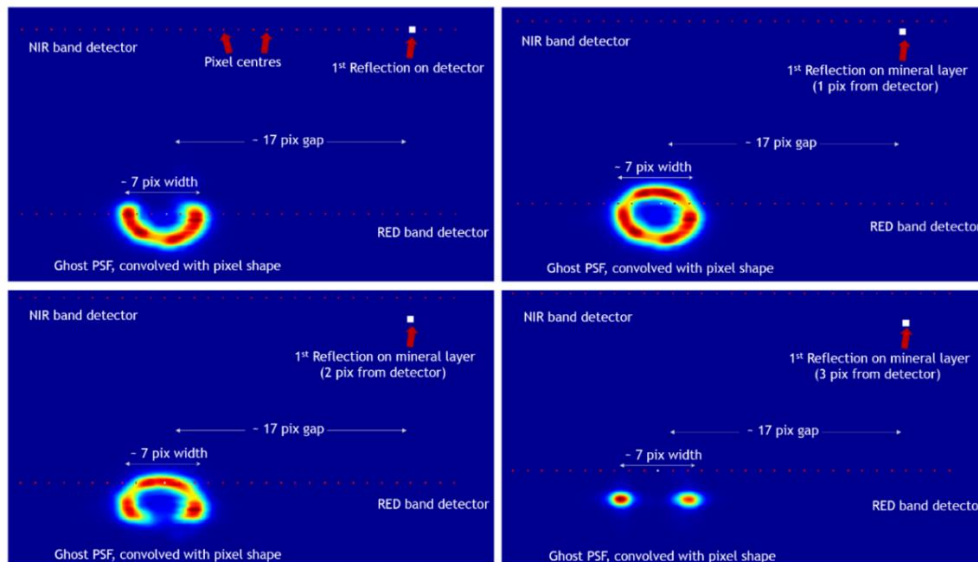


Figure 13. Computed ghost irradiance distributions for G_1 and the different G_2 ghost subpaths.

6. CROSS-TALK IMAGE MODELLING

In order to perform image simulations, it is necessary to derive a convolution mask that, when applied to a channel's image, reproduces the ghost effect on the image of the affected channel. In figure 13 is presented the image analysis performed to derive the mask coefficients at field point M_2 of the T2 camera, with NIR as the originating channel. In the

four figure's panels are displayed the computed FP irradiance distributions (after convolution with the pixel shape) for first reflections on the NIR detector line (G_1 ghost path), and on the detector coating (G_2 ghost path) at one, two and three pixels from the detector line, in the direction of the ghost affected line. Irradiance values and across-track distances between the location of the first reflection and the center of the ghost distribution have been tuned to reproduce the experimental results described in section 5.2.

The ghost irradiance distribution corresponds to a blurred version of the irradiance map at the telescope's exit pupil, with the central hole associated to the secondary mirror obscuration. The ring shape is trimmed in some cases by the narrow slits on the filter window, following a pattern that depends on the along-track position of the first reflection (on the detector line, or at different distances on the detector coating). At this field location, the centers of the ghost irradiance distributions are displaced across-track by 17 pixels, from the location of the first reflection on the CCD.

The mask coefficients could be readily determined by sampling the presented distributions at the pixel centers of the affected detector line. The only contributions are those associated to reflections on the detector line, and on the detector coating at one and two pixel distances. Each of them contribute to one row of the convolution mask, with the detector line coefficients in the central row. In figure 14 is presented as an illustration the mask obtained by application of this procedure.

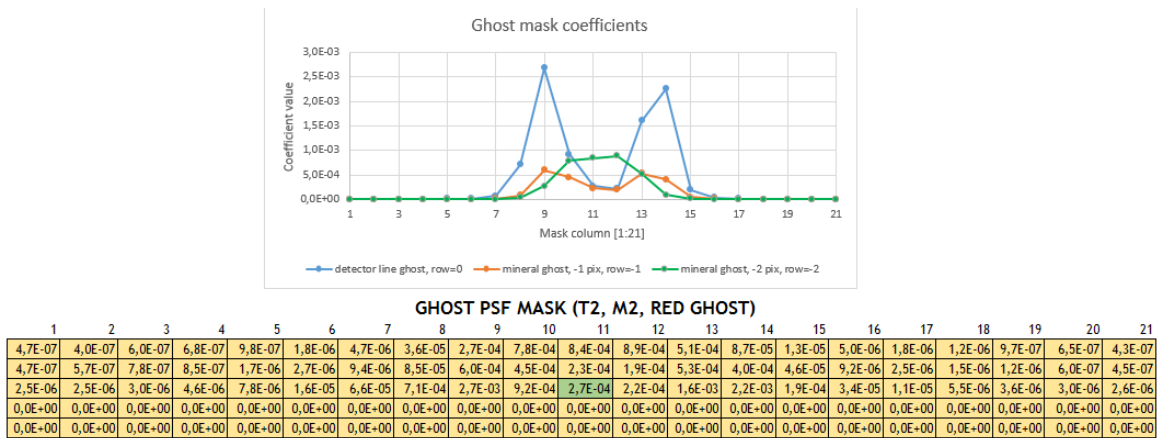


Figure 14. Derived convolution mask coefficients for field M₂ of the T₂ camera, with NIR as the ghost originating channel.

7. CROSS-TALK CORRECTION

As the studied ghost is a space-variant degradation, computation of the ghost image for a given channel requires previous determination of the convolution masks and across-track displacements at different field positions, together with an interpolating scheme to enforce image data continuity. Once the ghost images have been simulated for the three originating channels (blue, green and NIR), their effect can be removed by subtracting them from the images of the ghost-affected channels (green, NIR and red, respectively).

As an initial performance test, the convolution mask derived in section 6 has been used to simulate and then remove the image ghost on the red channel of an actual image acquired with the T₂ camera, containing relevant information around the modeled M₂ field point. The processed image was acquired during the stray-light tests performed on that camera and field point (see section 5.1), and was not used in the tuning of the correction method parameters. The square shape obtained from the measurement is displayed (black solid line) in the left panel of figure 15, where the ghost-induced bumps and depressions are clearly visible. These artifacts have been completely removed (dashed red line) after application of the devised ghost-correction procedure. In the right panel of the figure are presented the results at the square's right edge in a semi-logarithmic plot, with reference to achieved stray-light rejection factors.

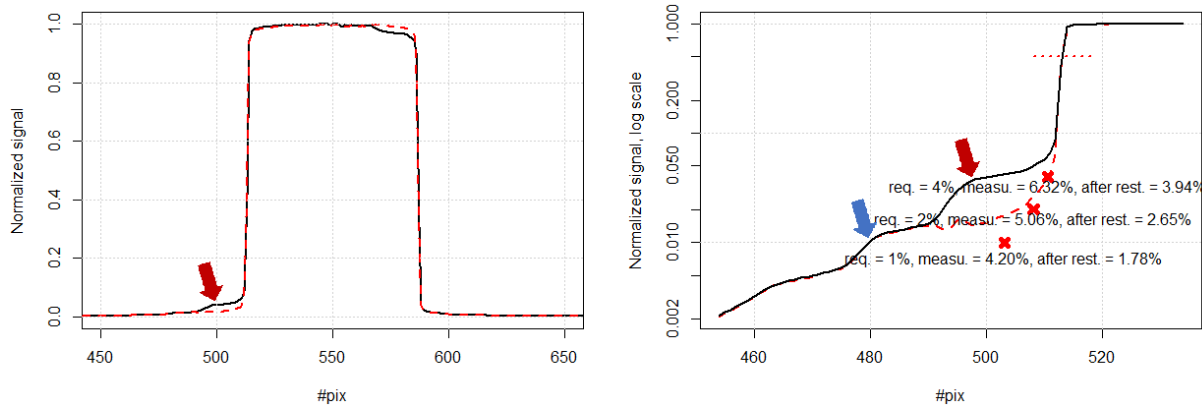


Figure 15. Ghost correction results on the red channel of a square image. Left: original ghost-affected image (black) and results (red) after application of the ghost correction algorithm; right: semi-logarithm plot, with stray-light rejection levels before (black) and after (red) application of the correction.

As can be seen, application of the ghost-correction process has removed the signal bump associated to the studied ghost almost completely, maintaining other features (such as the smaller bump associated to a 4-reflection path) unaltered. Stray-light rejection levels have been reduced in a range from 40% to 60%, with larger improvements occurring at longer distances from the edge. Taking left edge stray-light rejection levels as representative of achievable values in complete ghost absence, it can be concluded that the devised ghost characterization and correction method is able to reduce the aggregated ghost contribution in a range from 60% to 75%, with better performance also here at longer distances from the edge.

REFERENCES

- [1] Miravet C., Zorita D., Santos C., Sánchez J. et al, “Correlation of INGENIO/SEOSAT radiometric model with the results of the radiometric campaigns”, Proc. SPIE 10562, International Conference on Space Optics — ICSO 2016, (2017).
- [2] Taubmann, G., Arroyo J.M., Miravet C., Zorita D. et al, “Finite element model assisted shimming of INGENIO/SEOSAT primary mirrors”, Proc. SPIE 10562, International Conference on Space Optics — ICSO 2016, (2017).
- [3] Marini. A., Reina Barragan F.J., Crippa G., Harnisch B. et al, “SEOSAT/INGENIO - a Spanish high-spatial-resolution optical mission”, Proc. SPIE 10563, International Conference on Space Optics — ICSO 2014, (2017).
- [4] Miravet C., Zorita D., Bueno J.I., Pascual L. et al, “Development status of the telescope for the Ingenio/SEOSAT mission primary payload”, Proc. SPIE 8167, Optical Design and Engineering IV, (2011).
- [5] Pascual L., Bueno J.I., Zorita D., Miravet C. et al, “Detailed Optical Design of SEOSAT/Ingenio Spanish High Resolution Imaging Instrument”, International Conference on Space Optics — ICSO 2012.
- [6] Zorita D., Miravet C. and Bueno J.I., “Challenges and developed solutions for the principal payload of the SEOSAT/Ingenio mission”, RAQRS III, Recent Advances in Quantitative Remote Sensing, (2010).